Coherent structures emerging from turbulence in the nonlocal complex Ginzburg-Landau equation

Vladimir García-Morales,[1,*] Robert W. Hölzel,[1] and Katharina Krischer[1]
[1]*Physik-Department E19, Technische Universität München, James-Franck-Strasse 1, D-85748 Garching, Germany*
(Received 31 March 2008; published 28 August 2008)

The nonlocal complex Ginzburg-Landau equation (NCGLE) has been recently derived as a general model for electrochemical systems close to a supercritical Hopf bifurcation [V. Garcia-Morales and K. Krischer, Phys. Rev. Lett. **100**, 054101 (2008)]. We carry out the stability analysis of plane waves for arbitrary Fourier numbers providing the generalized Eckhaus criterion for stability to long-wavelength fluctuations in the NCGLE. We also show that coherent structures (standing waves, heteroclinic orbits) arise in the NCGLE at intermediate coupling ranges from states which are turbulent under local coupling. These results are substantiated through simulations of the full NCGLE and bifurcation analysis of the truncated NCGLE which preserves the symmetry of the observed patterns. We briefly discuss the effect of the nonlocal coupling on other localized structures (Bekki-Nozaki holes) found in the NCGLE.

DOI: 10.1103/PhysRevE.78.026215 PACS number(s): 05.45.−a, 82.40.Bj, 47.54.−r

I. INTRODUCTION

The complex Ginzburg-Landau equation (CGLE) constitutes a general model for spatially extended oscillatory nonlinear systems [1,2] in which the spatial coupling between oscillators is diffusive and, therefore, described by a (local) Laplacian operator. The CGLE has an extremely rich and complicated behavior and has been the subject of intense study in the past two decades. It is a useful model for the dynamics of oscillatory reaction-diffusion systems and allows one to describe the essentials of spatiotemporal chaos and turbulent states which arise when the uniform oscillation loses stability to a set of oscillating Fourier modes [3]. It also describes spatially coherent structures [4–6] which are in turn regarded as building blocks for spatiotemporal intermittency. When fully rescaled, the CGLE depends only on two essential parameters, c_1 and c_2, which can be calculated from the actual homogeneous dynamics of any oscillatory system close to a supercritical Hopf bifurcation (SHB). This calculation is in general very cumbersome for systems with more than two components.

Despite such generality, the CGLE cannot rigorously describe the behavior of systems under nonlocal coupling (NLC). For example, globally coupled systems [7] fall into this category. In certain surface reactions, this all-to-all coupling is produced through interactions with the gas phase, where rapid mixing is realized [8] prompting studies on the globally coupled CGLE [7]. Yet, another general situation is not captured with this ansatz, namely, spatial coupling with an arbitrary coupling range. Normal forms with nonlocal kernels are of great interest to many branches of physics [9]. Already more than one decade ago, Kuramoto [10] formulated a nonlocal CGLE for a class of three (or more) component reaction-diffusion systems by means of an extended center manifold reduction in which the coupling of the oscillators, although nonlocal, was explicitly assumed to be weak. The latter assumption makes center-manifold theory (a local method) suitable also to deal with nonlocal interactions. Such an approach allows one to describe patterns with characteristic lengths comparable to the effective radius of the coupling. As pointed out recently by Kuramoto and Tanaka [11] the idea of introducing a weak, nonlocal coupling lies behind multiple bifurcation theory, which aims to capture such complex dynamics as is absent in the vicinity of a simple bifurcation point. Novel dynamical states, such as multiaffine turbulence [12] and chimera states [13] were found in the simulations. However, despite its possible relevance to reaction-diffusion systems of three or more components the nonlocal CGLE introduced in [11] is not directly related to any experimental system.

NLC arises naturally in electrochemical systems because of the long range influence of the electric potential, an additional relevant dynamical variable besides (and coupled to) chemical variables. At a given point, the effect of any inhomogeneity in the electric potential decays with $\sim 1/r$, where r is the distance to a reference position, coupling in this way an extended range of locations. This NLC, also called migration coupling, is synchronizing, and tends to smooth out any potential gradient parallel to the working electrode (WE) in absence of any nonlinear reaction kinetics [15]. The range of the coupling is determined by the aspect ratio $\beta \equiv w/L$, where L is the length of the WE [16,17] and w is the distance between the WE and the counterelectrode (CE). A nonlocal complex Ginzburg-Landau equation (NCGLE) has been very recently derived [14] as a general model for electrochemical oscillators. The NCGLE is a partial integrodifferential equation since the spatial coupling can no longer be specified by a Laplacian operator as in the CGLE but rather by an integral operator containing a nonlocal kernel. The NCGLE reads [14]

$$\partial_t W = W - (1 + ic_2)|W|^2 W + (1 + ic_1) \times \int_{WE} H_\beta(|x - x'|)[W(x') - W(x)]dx', \qquad (1)$$

where W is the (complex) amplitude, c_1 and c_2 are dimen-

*vmorales@ph.tum.de

sionless parameters that can be calculated from the homogeneous dynamics accompanying the nonlocal and nonlinear terms, respectively, and β is the coupling range, the new essential parameter of the NCGLE when compared to the CGLE. β controls both the range and the normalization of the nonlocal kernel $H_\beta(|x-x'|)$. The latter couples two different positions x and x'. On a 1D ring electrode it is given by [18]

$$H_\beta(|x-x'|) = \frac{\pi}{4\beta^2 \sinh^2\left(\frac{\pi(x-x')}{2\beta}\right)} + \frac{\delta(|x-x'|)}{\beta}. \quad (2)$$

The CGLE is regained from the NCGLE when $\beta \to 0$, i.e., for vanishing coupling range (local coupling limit). Although the NCGLE can be extended to some 2D electrodes, it was derived explicitly for one-dimensional (1D) ring electrodes because of their enormous experimental interest [15–19]. The NCGLE was also successfully mapped to a two-component system of experimental interest: an N-type negative differential resistance electrochemical oscillator [19] in the vicinity of a SHB [14]. Even in the absence of any diffusing species, this system was shown to exhibit (electrochemical) turbulence for wide parameter ranges. In [14], it was also pointed out that the effect of the NLC in electrochemical systems is creating structures of longer wavelength as well as compressing the band of unstable wave numbers. In fact, the length of the structures is comparable to the coupling radius, which can be tuned experimentally by changing β.

The aim of this paper is twofold: (1) to extend the stability results on the uniform oscillation of [14] to plane waves with arbitrary wave number and (2) to describe some coherent solutions that we have found in the NCGLE in the turbulent regime which include standing waves and robust heteroclinic orbits between fixed points or limit cycles. The structure of the paper is as follows. In Sec. II we briefly explain how the NLC arises in electrochemical systems and we describe several properties that allow one to derive the NCGLE, analyzing also its asymptotic behavior. In Sec. III, we carry out the linear stability analysis of plane waves for an arbitrary Fourier number, deriving the generalized Eckhaus criterion for the NCGLE. This allows us to determine the band of stable plane waves in the Benjamin-Feir (BF) stable regime elucidating the effect of the NLC in this multistability regime. Finally, in Sec. IV, we show the existence of coherent structures in the NCGLE within the BF unstable regime and substantiate our observations by means of bifurcation analysis. We conclude with some brief remarks on other behaviors observed, which are of relevance to the study of localized structures that were also found in the CGLE.

II. NONLOCAL COUPLING IN 1D ELECTROCHEMICAL SYSTEMS AND THE NCGLE

In the following we consider a 1D ring working electrode immersed in an electrolyte solution at a vertical position $z=z_{WE}$ and a CE at position $z=z_{WE}+w$. For simplicity we take $z_{WE}=0$. Our starting point is the dynamics for the double layer potential ϕ_{DL} which comes from the differential charge conservation law at the interface [15]

$$-\sigma \frac{\partial \phi(\mathbf{r},t)}{\partial z}\bigg|_{z_{WE}} = C\frac{\partial \phi_{DL}(\mathbf{r},t)}{\partial t} + i_F(\mathbf{r},t), \quad (3)$$

where $\mathbf{r}=(x,z)$ is the position vector containing the coordinates parallel x and perpendicular z to the WE, $\phi(\mathbf{r},t)$ is the electric potential in the electrolyte [15,17], C is the capacitance of the double layer, σ is the dimensionless conductivity, and i_F is the Faradaic current, which couples the dynamics of ϕ_{DL} to the electrochemical kinetics at the interface. The differential term on the left-hand side of Eq. (3) is the local electric current density reaching the electrode from the electrolyte. When the potential distribution is homogeneous, the latter term takes the form

$$-\sigma \frac{\partial \phi(\mathbf{r},t)}{\partial z}\bigg|_{z_{WE}} = \frac{\sigma}{w}\phi\bigg|_{z_{WE}}, \quad (4)$$

where we have taken, for simplicity, that the potential at the CE is zero. If U is the external voltage applied, the double layer potential is then defined in terms of $\phi|_{z_{WE}}$ as

$$\phi_{DL} = U - \phi|_{z_{WE}}. \quad (5)$$

In case of an inhomogeneous potential distribution, the deviation from homogeneity can be expressed as

$$i_{\text{mig. coupling}} = -\sigma \left(\frac{\partial \phi}{\partial z} + \frac{\phi}{w}\right)\bigg|_{z_{WE}}, \quad (6)$$

which provides the spatial coupling through the electric field in electrochemical systems. For a given size of the WE, w determines the *range of the coupling* which is a measure of the characteristic distance over which a change in the state at a particular position instantaneously affects neighboring parts. The dynamics of the double layer potential coming from Eq. (3) is usually coupled to the homogeneous reaction kinetics governing the evolution of a vector of chemical species $\mathbf{c}$ and can be written as [16]

$$\partial_t \phi_{DL} = f(\phi_{DL},\mathbf{c}) - \sigma \left(\frac{\partial \phi}{\partial z} + \frac{\phi}{\beta}\right)\bigg|_{z_{WE}}, \quad (7)$$

$$\partial_t \mathbf{c} = \mathbf{g}(\phi_{DL},\mathbf{c}), \quad (8)$$

where $f(\phi_{DL},\mathbf{c})$ and $g(\phi_{DL},\mathbf{c})$ are (vector) functions specifying the homogeneous dynamics and we have made the transformations $t \to Ct$ and $z \to zL$.

As shown in [18], we can express the NLC Eq. (6) in a more convenient form by means of a Green's function as

$$i_{\text{mig. coupling}} = -\sigma \left(\frac{\partial \phi}{\partial z} + \frac{\phi}{\beta}\right)\bigg|_{z_{WE}} = \sigma \int_{-\infty}^{\infty} H_\beta(|x-x'|)[\phi_{DL}(x') - \phi_{DL}(x)]dx', \quad (9)$$

with $H_\beta(|x-x'|)$ given by Eq. (2). The derivation is given in

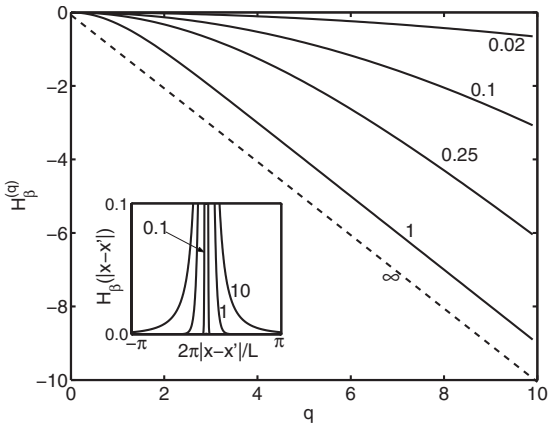

FIG. 1. Nonlocal kernel in Fourier space vs wave number q for the values of β indicated in the graph. Inset: $H_\beta(|x-x'|)$ calculated from Eq. (2) for $L=20$.

the Appendix for completeness. Through this approach the migration coupling does not depend on $\phi(x,z)$ and therefore Eq. (3) is mathematically closed in terms of $\phi_{DL}(x)$. This is the nonlocal kernel for 1D electrochemical systems. A crucial quantity in deriving the NCGLE is the Fourier transform of Eq. (2) given by

$$H_\beta^{(q)} = -q\coth(q\beta) + \frac{1}{\beta}, \tag{10}$$

where $q \equiv \frac{2\pi n}{L}$. This expression is plotted in Fig. 1 for several β values. In the limit $\beta \to 0$ the NLC becomes local (diffusionlike, $\sim q^2$) with "diffusion coefficient" $\sigma\beta/3$. In physical space the kernel becomes

$$H_{\beta\to 0}(|x-x'|) = \frac{\beta}{3}\delta^{(2)}(x'-x), \tag{11}$$

where $\delta^{(2)}(x'-x)$ denotes the second derivative of the Dirac delta function. The nth order derivative of the latter has the following property:

$$\int_{-\infty}^{\infty} \delta^{(n)}(x'-x)f(x')dx' = (-1)^n \partial_x^n f(x), \tag{12}$$

where $f(x)$ is a suitable test function. Therefore, in physical space and in the limit $\beta \to 0$ the NLC Eq. (9) takes the form

$$i_{\text{mig. coupling}} = \frac{\sigma\beta}{3}\partial_x^2 \phi_{DL}(x). \tag{13}$$

If, on the contrary, we consider the infinite coupling range limit $\beta \to \infty$, Eq. (10) now gives $H_{\beta\to\infty}^{(q)} = -|q|$ and in physical space we have

$$H_{\beta\to\infty}(|x-x'|) = \frac{1}{\pi|x-x'|^2}. \tag{14}$$

Distant points are now coupled to each other and the coupling can have a global contribution as shown in the inset in Fig. 1.

A system close to a supercritical Hopf bifurcation is in a situation in which two conjugate eigenvalues become critical, crossing the imaginary axis in the λ-μ plane, where μ is a control parameter that controls the onset of the oscillations (at $\mu=0$). In a spatially extended system, the NLC provides indeed a branch of eigenvalues λ_n that can be infinitesimally close to the critical one for infinite systems. The shift in the position of the eigenvalues caused by the NLC in the λ-μ plane with respect to the critical one (dictated by the homogeneous dynamics) is given by $H_\beta^{(q)}$ which is of order $\sim 1/L$ and $\sim 1/\beta$ [14] for $n \sim 1$. It is clear then that if we make an expansion around $\mu=0$ for finite although vanishingly small μ, the eigenvalues that are relevant to the critical dynamics fall in a circle of radius $|\mu| \equiv \varepsilon^2$ to which β and L must compare. Then, it is reasonable to introduce scaled variables $\tilde{x}=|\mu|x$ and $\tilde{z}=|\mu|z$ (and consequently $\tilde{L}=|\mu|L$ and $\tilde{\beta}=|\mu|\beta$). This contrasts with the diffusion coupling in which the scaling has the form $\tilde{x}=|\mu|^{1/2}x$ [1] coming from the dispersion relationship of the diffusion coupling which goes as $\sim 1/L^2$. Working with these scaled variables we have

$$\int_{-\infty}^{\infty} H_\beta(|x-x'|)(\ldots)dx' = \varepsilon^2 \int_{-\infty}^{\infty} H_{\tilde{\beta}}(|\tilde{x}-\tilde{x}'|)(\ldots)d\tilde{x}', \tag{15}$$

i.e., the integral operator for the NLC contributes at second order in the perturbation expansion: The nonlocal coupling is small and can be balanced at third order when the full expansion is considered [14]. This, indeed, makes applicable the center-manifold reduction method [11] while preserving at the same time nonlocal effects, absent in the CGLE [1]. When performing a perturbation expansion up to third order and rescaling all the quantities we arrive at the standard form of the NCGLE, Eq. (1).

When $\beta \to 0$ the NCGLE becomes the CGLE through a "diffusion coefficient" $\beta/3$,

$$\partial_t W = W + (1+ic_1)\frac{\beta}{3}\partial_x^2 W - (1+ic_2)|W|^2 W.$$

The factor $\beta/3$ is nonessential in this limit (i.e., β and x are no longer independent) and can be absorbed in the spatial scaling by making the transformation $x \to \sqrt{\beta/3}x$. Since $\beta \to 0$, this is equivalent to considering an infinitely large system. We obtain in this case the CGLE

$$\partial_t W = W + (1+ic_1)\partial_x^2 W - (1+ic_2)|W|^2 W. \tag{16}$$

In the limit of large coupling range $\beta \to \infty$, the coupling can have a global contribution. However, it is to be noted that since $H_{\beta\to\infty}^{(0)} = 0$ the spatial average of the amplitude $\langle W \rangle$ does not contribute to the coupling and, hence, the NLC in this limit is mathematically different than the one in the globally coupled CGLE [7].

The latter asymptotic behavior of the NCGLE helps in understanding the role of nonlocality in the observed spatiotemporal patterns and its relationship to their characteristic length l_p. In general, from the dimensional argument involved in the derivation of the NCGLE, $l_p = O(r_0/|\mu|)$, where r_0 is the effective coupling radius. In the limit β small $r_0 \sim \sqrt{\sigma\beta/3}$ and, as the Hopf bifurcation is approached ($|\mu| \to 0$), l_p grows as $|\mu|^{-1}$ and r_0 falls well within the scale

of l_p. Consequently, in this limiting situation the local coupling arises. When β is, however, intermediate or large, the coupling radius scales as $r_0 \sim \sigma|\mu|$ and l_p becomes independent of $|\mu|$. In this more general case nonlocal effects are preserved close to criticality and, at the same time, make possible the extended center manifold reduction on which the NCGLE is built. Most remarkably, the behavior of the coupling radius is entirely dictated by β and no assumptions on weak coupling need to be made as in [11], since the weakness of the coupling is automatically warranted by the property in Eq. (15) that the nonlocal kernel of electrochemical systems satisfy, as first pointed out in [14].

III. STABILITY ANALYSIS OF PLANE WAVES

The NCGLE, Eq. (1), admits as solution the oscillation

$$W_Q = a_Q e^{i(Qx-\omega_Q t)}, \tag{17}$$

with

$$|a_Q|^2 \equiv 1 - Q\coth(\beta Q) + \frac{1}{\beta} = 1 + H_\beta^{(Q)}, \tag{18}$$

$$\omega_Q \equiv c_2(1 + H_\beta^{(Q)}) - c_1 H_\beta^{(Q)}, \tag{19}$$

where $H_\beta^{(Q)} = -Q\coth(\beta Q) + \frac{1}{\beta}$. As done with the CGLE [1], we study the stability of plane waves of Fourier number Q by perturbing the NCGLE. By putting $W \approx [a_Q + u(x,t)]e^{i(Qx-\omega_Q t)}$ in Eq. (1) and neglecting terms in the perturbation $\sim uu$, $\sim u\bar{u}$, $\sim \bar{u}\bar{u}$ (the bar denotes complex conjugation) from second order on, we obtain

$$\begin{aligned}\partial_t u = &-(1+ic_1)H_\beta^{(Q)}u - (1+ic_2)(1+H_\beta^{(Q)}) \\ &\times[u+\bar{u}] + (1+ic_1)\int_{WE} H_\beta(|x-x'|) \\ &\times[u(x')e^{iQ(x'-x)} - u(x)]dx'.\end{aligned}$$

The complex conjugate of this equation takes the form

$$\begin{aligned}\partial_t \bar{u} = &-(1-ic_1)H_\beta^{(Q)}\bar{u} - (1-ic_2)(1+H_\beta^{(Q)}) \\ &\times[u+\bar{u}] + (1-ic_1)\int_{WE} H_\beta(|x-x'|) \\ &\times[\bar{u}(x')e^{iQ(x-x')} - \bar{u}(x)]dx'.\end{aligned}$$

If we do the Fourier transform of the latter equation and apply the convolution theorem, we obtain for the mode with wave number q,

$$\partial_t \begin{pmatrix} u_q \\ \bar{u}_q \end{pmatrix} = \begin{pmatrix} L_{11} & L_{12} \\ L_{21} & L_{22} \end{pmatrix} \begin{pmatrix} u_q \\ \bar{u}_q \end{pmatrix}, \tag{20}$$

where

$$L_{11} = -(1+ic_2)(1+H_\beta^{(Q)}) + (1+ic_1)(H_\beta^{(q+Q)} - H_\beta^{(Q)}),$$

$$L_{12} = -(1+ic_2)(1+H_\beta^{(Q)}), \quad L_{21} = \overline{L_{12}},$$

$$L_{22} = -(1-ic_2)(1+H_\beta^{(Q)}) + (1-ic_1)(H_\beta^{(q-Q)} - H_\beta^{(Q)}),$$

and u_q and $\bar{u}_q$ are the Fourier transforms of u and $\bar{u}$, respectively. The diagonalization of the matrix on the right-hand side of Eq. (20) yields a characteristic equation of the form

$$\lambda^2 + (r_1 + ir_2)\lambda + (p_1 + ip_2) = 0, \tag{21}$$

where

$$r_1 = 2 + 4H_\beta^{(Q)} - H_\beta^{(q+Q)} - H_\beta^{(q-Q)},$$

$$r_2 = -c_1(H_\beta^{(q+Q)} - H_\beta^{(q-Q)}),$$

$$\begin{aligned}p_1 = &-(1+c_1c_2)(1+H_\beta^{(Q)})(H_\beta^{(q-Q)} + H_\beta^{(q+Q)} - 2H_\beta^{(Q)}) \\ &+ (1+c_1^2)(H_\beta^{(q+Q)} - H_\beta^{(Q)})(H_\beta^{(q-Q)} - H_\beta^{(Q)}),\end{aligned}$$

$$p_2 = (c_1 - c_2)(1 + H_\beta^{(Q)})(H_\beta^{(q-Q)} - H_\beta^{(q+Q)}). \tag{22}$$

An important quantity determining the stability of wave number Q against fluctuations of a given wave number q is

$$K_\beta(Q,q) = p_2^2 - r_1 r_2 p_2 - r_1^2 p_1. \tag{23}$$

Negative $K_\beta(Q,q)$ implies stability and positive $K_\beta(Q,q)$ instability. For the homogeneous wave number $Q=0$ we have

$$K_\beta(0,q) = -4(1 - H_\beta^{(q)})^2[(1+c_1^2)H_\beta^{(q)2} - 2(1+c_1c_2)H_\beta^{(q)}]. \tag{24}$$

Since $H_\beta^{(q)} < 0$ for $q \neq 0$, the homogeneous wave number can only be unstable if

$$\alpha = 1 + c_1c_2 < 0. \tag{25}$$

Therefore, the same condition as in the CGLE for the instability of the homogeneous wave number holds, $\alpha=0$ giving the BF line in the c_1-c_2 plane. When $\alpha<0$ there exists a band of Fourier modes that destabilize the homogeneous oscillation as discussed in [14] since in that case $K_\beta(0,q)>0$ for sufficiently small q below a critical value q_m that can be calculated from [14]

$$q_m\coth(q_m\beta) - \frac{1}{\beta} = \frac{2|\alpha|}{1+c_1^2}. \tag{26}$$

We can still ask whether there exist other plane waves which are stable to long-wavelength fluctuations, i.e., we study the stability for a plane wave Q to fluctuations in which $|q|$ is small. We can expand the dispersion relationship Eq. (10) in series around Q,

$$H_\beta(Q \pm q) \approx H_\beta^{(Q)} \pm qH_\beta^{(Q)\prime} + \frac{1}{2}q^2 H_\beta^{(Q)\prime\prime}, \tag{27}$$

with

$$H_\beta^{(Q)\prime} = \frac{dH_\beta^{(Q)}}{dQ} = -\coth(Q\beta) + Q\beta\sinh^{-2}(Q\beta),$$

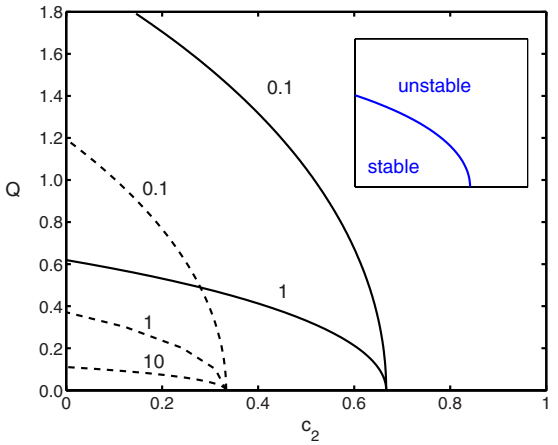

FIG. 2. (Color online) Curves separating regions of stable and unstable wave numbers (as sketched in the inset) calculated from Eq. (31) for $c_1=-3.0$ (dashed lines) and -1.5 (continuous lines) and for the values of β indicated besides each curve.

$$H_\beta^{(Q)\prime\prime} = \frac{d^2 H_\beta^{(Q)}}{d^2 Q} = 2\beta[1 - Q\beta \coth(Q\beta)]\sinh^{-2}(Q\beta). \tag{28}$$

If we replace these expressions in Eqs. (22) and (23) and retain only terms to q^2 we obtain

$$K_\beta(Q, q \approx 0) = (1 + c_1^2)H_\beta^{(Q)\prime 2} + (1 + c_1 c_2)(1 + H_\beta^{(Q)})H_\beta^{(Q)\prime\prime}, \tag{29}$$

since $H_\beta^{(Q)\prime\prime} < 0$ for $Q > 0$ (as shown in Fig. 1 $H_\beta^{(Q)}$ is concave) only for $\alpha > 0$ can plane waves exist with $Q \neq 0$ which are stable to long-wavelength fluctuations. Quite interestingly, for $Q \neq 0$, when $\beta \to \infty$ we have $H_\beta^{(Q)} = -|Q|$, $H_\beta^{(Q)\prime} = -Q/|Q|$, $H_\beta^{(Q)\prime\prime} = 0$ and therefore

$$K_{\beta\to\infty}(Q, q \approx 0) = 1 + c_1^2 > 0, \tag{30}$$

which implies that every plane wave with $Q \neq 0$ is unstable. This contrasts with the CGLE behavior for which there always exists a band of stable Fourier modes provided that $\alpha > 0$. In fact, as is clear from Fig. 2, the effect of increasing β is, for given c_1 and c_2, compressing the band of stable wave numbers. We plot in Fig. 2 the curves separating regions of stable and unstable wave numbers (below and above each curve, respectively, as sketched in the inset) as a function of c_2 and for different c_1 and β values (indicated in the figure). The point at which each curve intersects the c_2 axis with $|Q| = 0$ is dictated by the BF stability criterion $\alpha = 0$. The curves are calculated from the transcendent equation

$$(1 + c_1^2)H_\beta^{(Q_E)\prime 2} + (1 + c_1 c_2)(1 + H_\beta^{(Q_E)})H_\beta^{(Q_E)\prime\prime} = 0, \tag{31}$$

which provides the critical wave number Q_E below which all Fourier modes are stable. This is the generalized Eckhaus criterion for stability of plane waves in the NCGLE.

In the limit $\beta \to 0$, our NCGLE reproduces the CGLE and we obtain analogous expressions for the coefficients, Eqs. (22), to the ones provided by Kuramoto for that specific case (see Appendix A in [1]).

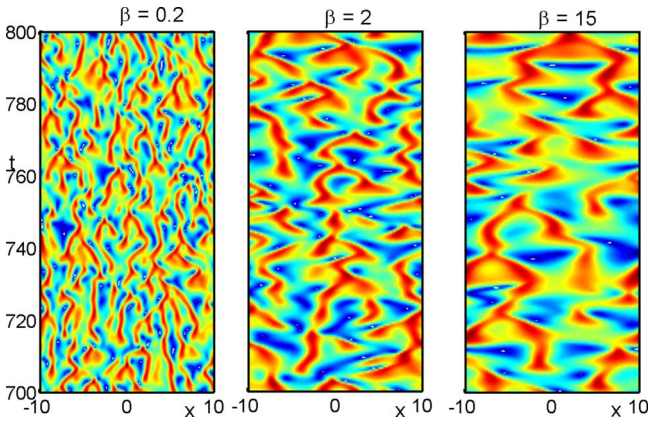

FIG. 3. (Color online) Spatiotemporal evolution of the modulus of the amplitude $|W|$ for $c_1=-2$, $c_2=2$, $L=20$, and the values of β indicated in the figure.

IV. COHERENT STRUCTURES IN THE NCGLE

An important feature of the NCGLE is that along with the coupling range also the characteristic lengths of the spatiotemporal structures increase [14]. This agrees with experimental findings [16]: In the defect turbulent region ($\alpha \ll 0$) larger structures and a lower density of spatiotemporal defects are observed for a larger coupling range. In Fig. 3 the spatiotemporal evolutions of the absolute value of the amplitude $|W|$ for three different β values in the BF unstable regime ($\alpha < 0$, $c_1=-2$, $c_2=2$) are shown. For all spatiotemporal patterns considered in this paper, the NCGLE was simulated by using a pseudospectral method with 700 Fourier modes, a system length $L=20$, periodic boundary conditions, and an exponential time stepping algorithm [20]. It is observed that as β is increased, the characteristic length of the spatiotemporal structures also increase. Through the linear stability analysis of the homogeneous solution, it was found [14] that the band of Fourier numbers that destabilize the uniform oscillation is both compressed and displaced to longer wavelengths. For sufficiently large coupling range, turbulence can even be suppressed beyond the BF stable regime in the NCGLE giving rise to spatially coherent structures.

A. Standing waves

An example of coherent structures that we found in the NCGLE are the standing waves shown in Fig. 4(a). The pattern possesses dihedral D_2 symmetry [21] at all times: it has two spatial reflection symmetry axes separated by $L/4$ (i.e., rotated $\pi/2$), and spatial frequency $q = 4\pi/L$. This symmetry is sketched in Fig. 5(a). The pattern is found for $\beta=2$ and parameter values in the BF unstable regime ($c_1=-4$, $c_2=0.9$). The solution shifts periodically $L/4$ in space. We can gain insight in this and other patterns if we make the projection

$$W(x,t) = \sum_{n=-\infty}^{\infty} W_n(t) e^{i2\pi n x/L} \tag{32}$$

onto the NCGLE, Eq. (1). Then, for the Fourier number n we obtain

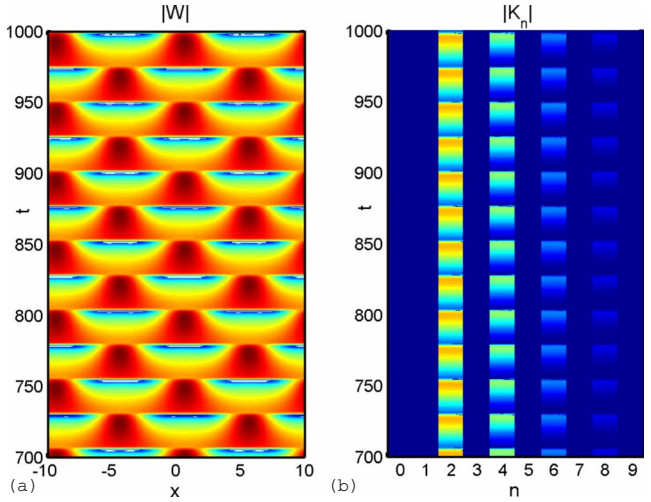

FIG. 4. (Color online) (a) Spatiotemporal evolution of the modulus of the amplitude $|W|$ for $c_1=-4$, $c_2=0.9$, $\beta=2$, and $L=20$. (b) Temporal evolution of $|K_n|$, computed from Eq. (34) for different wave numbers n.

$$\dot{W}_n = \left(1 + (1+ic_1)\left[-\frac{2\pi n}{L}\coth\left(\frac{2\pi n\beta}{L}\right) + \frac{1}{\beta}\right]\right) \times W_n - (1+ic_2)\sum_{j-k+l=n} W_j \bar{W}_k W_l. \tag{33}$$

In this representation, the NLC term reads

$$K_n \equiv (1+ic_1)\left(\frac{1}{\beta} - \frac{2\pi n}{L}\coth\frac{2\pi n\beta}{L}\right)W_n = (1+ic_1)H_\beta^{(2\pi n/L)}W_n. \tag{34}$$

It vanishes for any homogeneous state and is maximum for the relevant Fourier modes causing the inhomogeneity. The absolute value of this quantity as a function of n and time is, therefore, a useful means to characterize a spatiotemporal pattern in the NCGLE. We show in Fig. 4(b) the time evolution of $|K_n|$ for the standing wave pattern on the left. No odd Fourier modes contribute to the pattern, therefore the latter is invariant upon a $L/2$ translation even in the switching regions in which the $L/4$ spatial shifts occurs. A spatial translation of d, T_d acting on Fourier mode W_n is formally defined as the operation

$$T_d: W_n \to \exp(i2\pi nd/L)W_n. \tag{35}$$

As it is the case with the CGLE [22], the NCGLE is invariant under the action of the $\mathbb{S}^1$ phase symmetry γ: $W(x,t)\to W(x,t)e^{i\gamma}$ and the O(2) symmetry generated by invariances to translation T_d: $W(x,t)\to W(x-d,t)$ and reflection R_f: $W(x,t)\to W(-x,t)$. This also means that nontrivial solutions of the NCGLE exist on a two-torus with $\mathbb{S}^1\times$O(2) symmetry [22,23]. We can decouple the phase symmetry of the system [22,24] by writing $W_n=w_n e^{i\phi(t)}$. Then, by using the fact that w_0 is real, we have from Eq. (33),

$$\dot{w}_n + i\dot{\phi}w_n = [1+(1+ic_1)H_\beta^{(2\pi n/L)}]w_n - (1+ic_2)\sum_{j-k+l=n} w_j\bar{w}_k w_l, \tag{36}$$

where

$$\dot{\phi} = \mathrm{Im}\left(-\frac{1+ic_2}{w_0}\sum_{j-k+l=n} w_j\bar{w}_k w_l\right). \tag{37}$$

To describe the pattern in Fig. 4, and because of its manifest $T_{L/2}$ invariance and reflection symmetries, we can confine our study to the dynamics in the D_2 subspace. The dominant contributions to the pattern come from the homogeneous oscillation and the first even Fourier mode $n=2$ ($w_1=w_{-1}=0$ because of the overall D_2 symmetry). We can thus truncate the NCGLE to these three relevant modes w_0, w_2, and w_{-2}. Since in D_2 we further have $w_2=w_{-2}$, if we write $w_0=a_0$ and $w_2=w_{-2}=a_2+ib_2$, we obtain the following coupled set of real-valued differential equations:

$$\dot{a}_0 = a_0 - a_0^3 - 2a_0b_2^2 - 6a_2^2a_0 + 4c_2a_2b_2a_0,$$

$$\dot{a}_2 = a_2 + H_\beta^{(4\pi/L)}(a_2 - c_1b_2) - 3a_2a_0^2 - 7a_2b_2^2 - 3a_2^3 + c_2b_2^3 - 3c_2a_2^2b_2,$$

$$\dot{b}_2 = b_2 + H_\beta^{(4\pi/L)}(b_2 + c_1a_2) + 3c_2a_2^3 - 3b_2^3 - 2c_2a_2a_0^2 - b_2a_0^2 + b_2a_2^2 - c_2a_2b_2^2. \tag{38}$$

By this technique the uniform oscillation is reduced to the fixed point (1, 0, 0) in the phase space spanned by the variables (a_0,a_2,b_2). Equations (38) are invariant under a spatial shift of $L/4$ [i.e., $T_{L/4}$: $(a_0,a_2,b_2)\to(a_0,-a_2,-b_2)$]. Therefore, any linearization must also be invariant under this operation [23] and we expect steady bifurcations to be pitchforks that break this symmetry. If we linearize Eqs. (38) around the fixed point corresponding to the uniform oscillation $(a_0,a_2,b_2)=(1,0,0)$, we find the eigenvalues $\lambda_0=-2$, $\lambda_\pm=-(1-H_\beta^{(4\pi/L)})\pm\sqrt{1+c_1H_\beta^{(4\pi/L)}(2c_2+H_\beta^{(4\pi/L)}c_1)}$. One of these eigenvalues becomes positive at a critical value $\beta_{4\pi}$, which obeys the equation

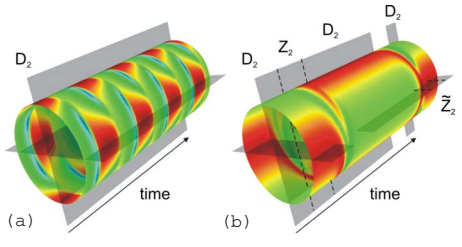

FIG. 5. (Color online) Sketch of the symmetries observed in the standing wave pattern [Fig. 4, (a)] and in the heteroclinic orbit between fixed points [Fig. 7, (b)]. D_2 is the dihedral group with two orthogonal reflection axes as indicated in the figure. Z_2 and $\tilde{Z}_2$ each have one reflection axis which is rotated $\pi/2$ with respect to each other. The D_2 symmetry (isomorphic to $Z_2\times\tilde{Z}_2$) is broken during the transitions between the equilibria in the pattern on the right.

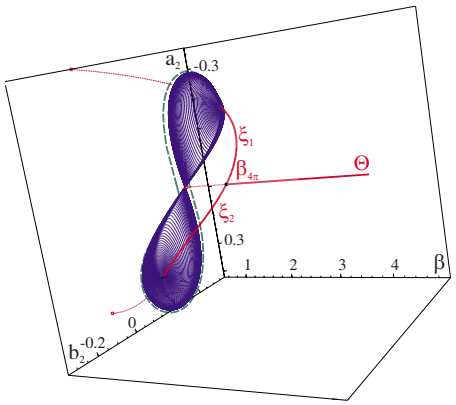

FIG. 6. (Color online) Bifurcation diagram of Eqs. (38) with β as the continuation parameter. Other parameter values are as in Fig. 4. At $\beta_{4\pi}$ a supercritical pitchfork bifurcation of the uniform oscillation Θ occurs and two states ξ_1 and ξ_2 emerge with the same stability. Shown also are the limit cycles found at lower β values. The thick dashed curve is a typical periodic trajectory found in the vicinity of the double saddle-loop point where both limit cycles meet.

$$\frac{4\pi}{L}\coth\left(\frac{4\pi\beta_{4\pi}}{L}\right)-\frac{1}{\beta_{4\pi}}=\frac{2|\alpha|}{1+c_1^2}. \tag{39}$$

For $\beta<\beta_{4\pi}$ the uniform oscillation is unstable to the first even wave number $q=4\pi/L$. Note that Eq. (39) is the same as Eq. (26) but solving there for β by taking $q_m=4\pi/L$. At $\beta=\beta_{4\pi}$ coming from higher values of β the uniform oscillation loses stability and two equilibria ξ_1 and ξ_2 related by a $L/4$ spatial shift (i.e., $T_{L/4}\xi_1=\xi_2$) emerge from a supercritical pitchfork bifurcation. In Fig. 6 we show the bifurcation diagram in three dimensions calculated with AUTO [25] with the real and imaginary parts of the first even wave number $n=2$ and the control parameter β. Other parameter values are as in Fig. 4. At $\beta_{4\pi}=2.75$ we observe the supercritical pitchfork bifurcation of the uniform oscillation and the two states emerging with a phase difference of π radians, in consistency with the phase shift of $L/4$ on the second Fourier mode. Eventually, at $\beta=2.17$, a supercritical Hopf bifurcation occurs and both branches bifurcate to stable limit cycles. Quite interestingly, the limit cycles meet in a double saddle-loop point [27] at $\beta\approx 2$ together with the unstable fixed point of the uniform oscillation. This explains the spatiotemporal pattern observed in Fig. 4. It is known that vector fields in the vicinity of a double saddle loop can have periodic orbits that lie close to the figure eight [27]. This is the case here, with each of the loops of the figure eight circling around the branch of a different quasiequilibrium which is spatially shifted by $L/4$. The spatiotemporal evolution of the full NCGLE (Fig. 4) is thus qualitatively captured by the three-mode truncation, the standing wave pattern being described by a trajectory similar to the thick dashed curve in Fig. 6.

B. Heteroclinic orbits

In Fig. 7(a) we show another coherent structure that arises in the NCGLE with a moderately large coupling range $\beta=3.5$, and parameter values in the BF unstable regime

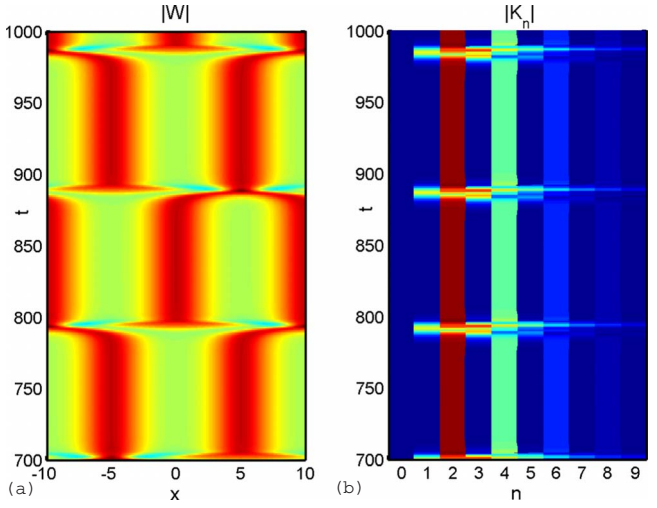

FIG. 7. (Color online) (a) Spatiotemporal evolution of the modulus of the amplitude $|W|$ for $c_1=-3$, $c_2=1$, and $\beta=3.5$. (b) Temporal evolution of $|K_n|$, computed from Eq. (34), for different wave numbers n.

($c_1=-3$, $c_2=1$). Here, the system changes aperiodically in time in an alternating manner between two states that represent stationary periodic structures. In Fig. 7(b), the time evolution of $|K_n|$ is plotted for the pattern on the left. It is observed that the odd Fourier wave numbers contribute here in shifting aperiodically the system $\pm L/4$. This behavior is characteristic of heteroclinic dynamics [26]. It was observed in the Kuramoto-Sivashinsky equation [28] and, recently, in the CGLE [22] although the patterns found in the latter work have a period two orders of magnitude smaller than the ones here. Furthermore, in Ref. [22], the CGLE is written in the form

$$\partial_t W = RW + (1+ic_1)\partial_x^2 W - (1+ic_2)|W|^2 W, \tag{40}$$

and the behavior found is discussed as a function of the parameter R. This parameter can be absorbed in the CGLE, however, through the scalings $t\to t/R$, $s\to s/\sqrt{R}$, $W\to\sqrt{R}W$ that bring Eq. (40) to the standard form, Eq. (16). No such transformations are possible in our case for β, the latter being the new essential parameter peculiar to the NCGLE.

While resting at each one of the $\pm L/4$ spatially shifted equilibria the patterns possess again D_2 symmetry. The latter is broken, however, during the transitions between the equilibria. In Fig. 5(b) we sketch this symmetry breaking. In each transition, either one of the reflection axes of the D_2 symmetry is lost together with the $L/2$ translation invariance. The remaining symmetry is characterized by the reflectional groups Z_2 or $\tilde{Z}_2$ which each have only one reflection axis. For simplicity, and without loss of generality, we consider in the following that Z_2 makes reference to the spatial profile with reflection symmetry axis at angle $\theta=0$ and $\tilde{Z}_2$ refers to a symmetrical spatial profile with reflection axis at $\theta=\pi/2$ (i.e., separated a distance $L/4$). We can gain better insight in the heteroclinic cycles using the technique of phase decoupling considered above for the standing wave but introducing also the contribution of the first Fourier mode $W_{\pm 1}$ and,

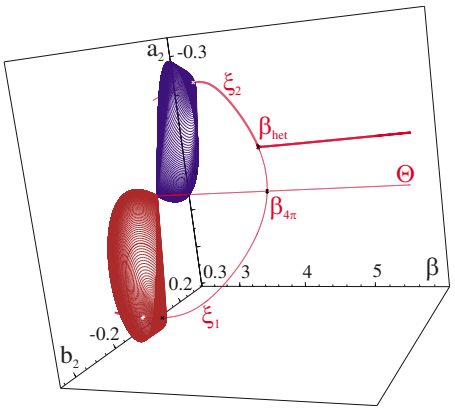

FIG. 8. (Color online) Bifurcation diagram of the five-mode truncation of the CGLE in the Z_2 even subspace with β as continuation parameter (other parameter values as in Fig. 7). Θ: uniform oscillation; ξ_1 and ξ_2: fixed points related by a $L/4$ spatial shift. Thick lines denote stable fixed points and thin lines denote unstable ones. $\beta_{4\pi}$ and β_{het} denote the location of the two pitchfork bifurcations where, respectively, $L/4$ symmetry is broken and ξ_2 gains stability. Limit cycles shown are stable in the ξ_2 branch and unstable in the ξ_1 one.

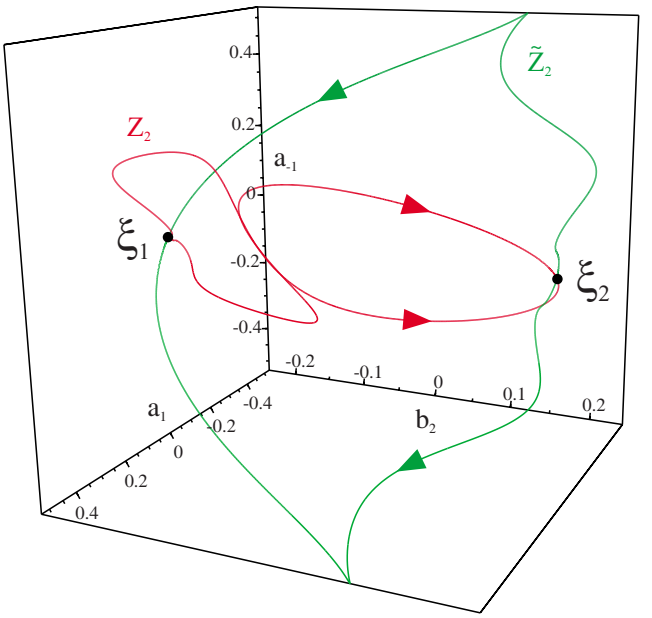

FIG. 9. (Color online) Heteroclinic orbits between the fixed points ξ_1 and ξ_2 through the orthogonal subspaces Z_2 and $\tilde{Z}_2$ obtained by simulating the full NCGLE. Parameter values as in Fig. 7.

therefore, considering a five-mode truncation of the NCGLE. In the "even" Z_2 and "odd" $\tilde{Z}_2$ subspaces, which are invariant to the corresponding reflection symmetries, the Fourier modes W_n with $n \neq 0$ satisfy the following relationships:

$$Z_2: \quad W_1 = W_{-1}, \quad W_2 = W_{-2}, \tag{41}$$

$$\tilde{Z}_2: \quad W_1 = -W_{-1}, \quad W_2 = W_{-2}. \tag{42}$$

Although the system is no longer confined only to D_2, as is the case with the standing wave, within this five-mode truncation we can understand the system dynamics as a switching between the equilibria in D_2 through either Z_2 or $\tilde{Z}_2$. In Fig. 8 we show the bifurcation diagram in the a_2-b_2 plane as a function of β in Z_2. It has a rather similar structure to the one found above for the standing wave (see Fig. 4), but there are also some important differences: the uniform oscillation is unstable for all β; both stationary states that emerge at $\beta_{4\pi}$ are thus also unstable but then one of them gains stability through a second pitchfork bifurcation at β_{het} while the other remains unstable; in the stable branch, a stable limit cycle emerges from a Hopf bifurcation, whereas an unstable one emerges from the Hopf in the unstable branch. Restricting the dynamics to the odd subspace $\tilde{Z}_2$ (not shown), where now $w_1 = -w_{-1}$ and $w_2 = w_{-2}$, the stability of the two different branches (and of the limit cycles) is the opposite. Thus, in the combined space, both equilibria ξ_1 and ξ_2 are saddle points, their unstable manifolds lying in Z_2 and $\tilde{Z}_2$, respectively, and the unstable ones in the respective orthogonal subspace. A robust heteroclinic orbit exists when there is a trajectory connecting the equilibria in both subspaces. With simulations of the full NCGLE for the parameter values as in Fig. 7 we show in Fig. 9 that this is indeed the case. In Fig. 9 the trajectory (with the decoupled phase) has been projected on the phase space spanned by the variables $a_1 - a_{-1}$ $-b_2$. We see that the orbit falls into two orthogonal planes connecting ξ_1 and ξ_2. These planes correspond each to the Z_2 and $\tilde{Z}_2$ subspaces where the $L/4$ spatial shift operation is implemented. Several initial conditions with noise were considered (a pulse, combinations of traveling waves with even and odd Fourier numbers) and, after a transient, the heteroclinic cycle in Fig. 7 was always attained.

We can ask whether there exists a relationship between the standing wave described in the previous section (see Fig. 4) and the heteroclinic orbits observed here for different values of c_1 and c_2. In Fig. 10 we plot the bifurcation diagram of the five-mode truncation in the Z_2 subspace in the a_0-β plane. As it is the case with the limit cycles in the standing wave pattern (see Fig. 6), the stable limit cycles here are connected to the unstable fixed point of the uniform oscilla-

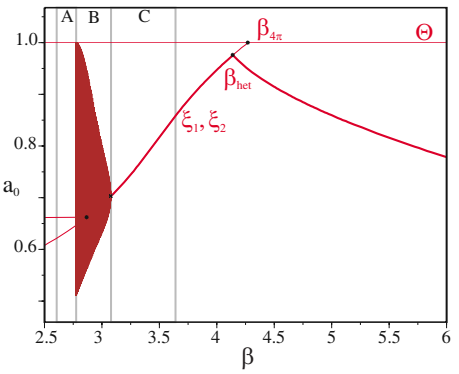

FIG. 10. (Color online) Projection of the bifurcation diagram shown in Fig. 8 in the a_0-β plane calculated with the five-mode truncation in the Z_2 subspace. Parameter values are as in Fig. 7. *A*, *B*, *C*, indicate the different regions in which the corresponding patterns of Fig. 11 are observed.

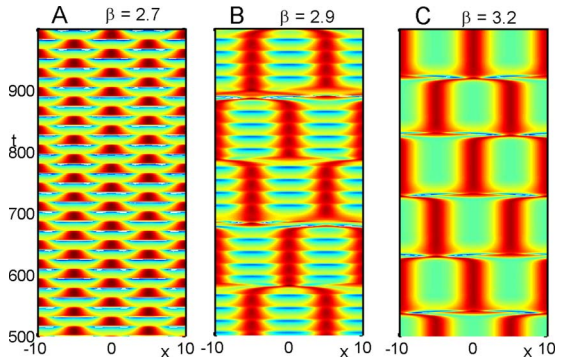

FIG. 11. (Color online) Spatiotemporal evolution of $|W|$ corresponding to the respective regions in the bifurcation diagram in Fig. 10. Other parameter values are as in Fig. 7.

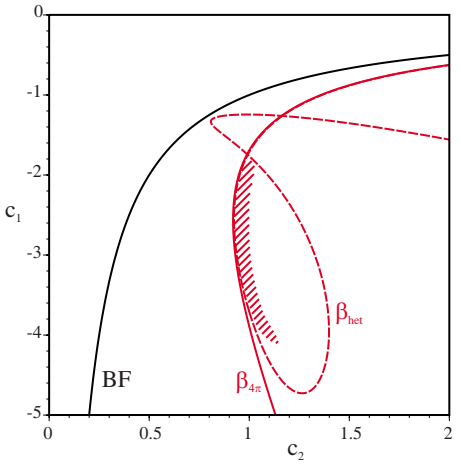

FIG. 12. (Color online) Pitchfork bifurcations that break the $L/4$ space symmetry ($\beta_{4\pi}$ curve) and that mark the onset to possible heteroclinic orbits (β_{het} curve) in the c_1-c_2 plane. The shadowed region is where robust heteroclinic orbits are found in the simulations with the full NCGLE. Shown also is the BF line ($\alpha=0$).

tion at $\beta \approx 2.76$. Two saddle limit cycles meet at this point, which is again a double saddle-loop point. A trajectory, with β lying in region A of the diagram, is closed and periodic, resembling the figure eight; hence each loop is $L/4$ spatially shifted. For the full NCGLE we again observe standing waves as in Fig. 6 which are robust to initial conditions. The heteroclinic orbits between fixed points of Figs. 7 and 9 obtained through simulations on the full NCGLE correspond to region C in Fig. 10. For β values in region B in Fig. 10 in the full NCGLE we find robust heteroclinic orbits between limit cycles, i.e., transitions between the limit cycles lying in D_2 whose stability is dictated by each subspace Z_2 and $\tilde{Z}_2$ with the phase symmetry decoupled. In Fig. 11 we plot the spatiotemporal evolution of $|W|$ with the full NCGLE for different β values and the same c_1 and c_2 as in Figs. 7–10. Pattern A corresponds to the standing wave and has overall D_2 symmetry [see Fig. 5(a)] as discussed above. When increasing β pattern B is found. It corresponds to the heteroclinic orbits between saddle limit cycles and at the transitions between the latter the random shifts of either $+L/4$ or $-L/4$ break the otherwise, overall $L/2$ translation symmetry of the pattern. During these transitions the symmetry is either Z_2 or $\tilde{Z}_2$. The overall solution is not periodic because the pattern shifts randomly $\pm L/4$ as a consequence of the two paths connecting ξ_1 and ξ_2 in each subspace Z_2 and $\tilde{Z}_2$ (see Fig. 9). Finally, in pattern C, at higher β the limit cycles disappear and the transitions are now between equilibria. "Limit cycles" and "equilibria" here make reference to the dynamical structures understood through the truncated NCGLE with the phase symmetry decoupled. Patterns B and C possess the same symmetries [see Fig. 5(b)].

While the pitchfork at $\beta_{4\pi}$ breaks the $L/4$ translation symmetry of the underlying dynamics (giving rise to two steady states that are $L/4$ spatially shifted but which are born exactly with the same properties and stability) the pitchfork at β_{het} changes the stability of one of the fixed points in each respective subspace allowing for the existence of heteroclinic orbits. The latter should exist in the full NCGLE for $\beta < \beta_{het}$ (see Fig. 10). In Fig. 12 we show the loci of both the $\beta_{4\pi}$ and β_{het} pitchfork bifurcations in the c_1-c_2 parameter plane. The shadowed region enclosed in the loop of the β_{het} line is where we found robust heteroclinic connections between fixed points in the simulations with the full NCGLE. These heteroclinic orbits, standing waves, etc. are robust coherent structures that exist in a region in which there is only defect turbulence under local coupling since their region of existence falls deep beyond the BF line in the unstable regime. Most remarkably, the coherent structures emerge because of the possibility of changing a physically meaningful and experimentally accessible parameter, the coupling range β at identical system length.

C. Other behaviors

The heteroclinic orbits in the previous section are only a few examples of coherent structures that can be found in the NCGLE. In this section we briefly mention other behaviors that we observe in the simulations. Another example of a coherent aperiodic structure is given in Fig. 13(b). The pat-

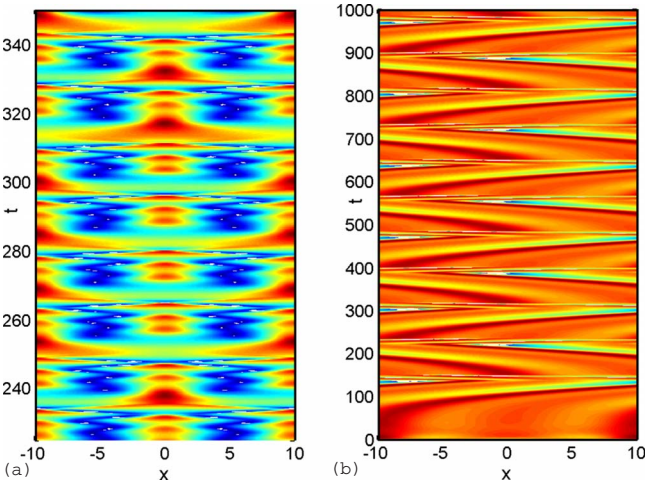

FIG. 13. (Color online) Spatiotemporal evolution of the modulus of the amplitude $|W|$ for $c_1=-6$, $c_2=1.5$, and $\beta=10$ (a) and $c_1=-3.0$, $c_2=0.9$, and $\beta=5$ (b).

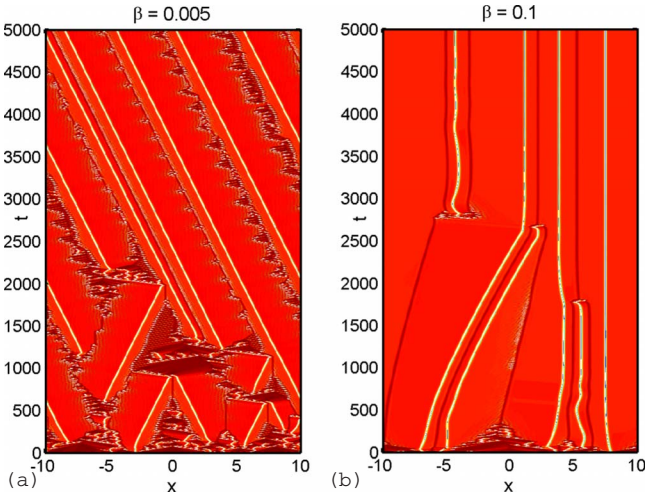

FIG. 14. (Color online) Spatiotemporal evolution of the modulus of the amplitude $|W|$ for $c_1=0$, $c_2=1.5$ and the values of β indicated in the figure. White lines are BNHs.

tern observed connects dynamical states that are this time $L/2$ spatially shifted and for which the first wave number provides the most important contribution. Another pattern that it is also $L/2$ spatially shifted but for which now the uniform oscillation has the most important contribution, is shown in Fig. 13(a). In this pattern the $L/2$ spatial shift involves one amplitude defect.

The CGLE is known to have localized solutions [5], the Bekki-Nozaki holes (BNHs) [4,29] being a well known example. The BNHs are localized dips in the amplitude W and usually have an associated "shock" (a localized maximum in the amplitude). These solutions connect two plane waves with wave numbers q_1 and q_2 by a localized object moving at velocity $v=(c_1-c_2)(q_1+q_2)$ [2]. Besides the so-called homoclons, these solutions are regarded as important building blocks of spatiotemporal intermittency [6]. When a hole and a shock collide, the shock can be either scattered or annihilated. Hole-shock pairs can also be generated as the result of annihilating shocks [30]. Since the NCGLE becomes the CGLE in the limit $\beta\to 0$, BNH solutions are also solutions of the NCGLE in at least that limiting case and for a range of finite nonvanishing values of β. We have simulated the NCGLE for parameter values lying in a region in which BNHs are known to be stable from the linear stability analysis carried on the CGLE [2,31]. The results are shown in Fig. 14 for $c_1=0$, $c_2=1.5$, and different values of β. We find that for very low β [Fig. 14(a)] we have stable BNHs that can propagate at a finite nonvanishing velocity as it is observed in the CGLE. As β is increased a grid of standing BNHs ($v=0$ holes) arises [Fig. 14(b)]. For β even higher, no BNHs exist and the uniform oscillation is stable. The behavior at β sufficiently high is similar to the one observed for the quintic CGLE with a negative coefficient $-\delta|W|^4W$ ($\delta>0$) [30], the only stable BNHs being standing holes.

V. CONCLUSIONS

In this paper we have studied several features of the NCGLE. This equation has been derived recently [14] as a general model to describe the dynamics of electrochemical systems close to a supercritical Hopf bifurcation. By means of the linear stability analysis of plane waves of arbitrary wave number to long-wavelength perturbations, we have derived the generalized Eckhaus criterion that holds for the NCGLE. The new essential physical parameter entering in the NCGLE, the coupling range β, allows one to tune the width of the band of stable plane waves in the BF stable regime. We find that in the limit $\beta\to\infty$ all plane waves are unstable. Although the NLC does not fully stabilize the uniform oscillation in the BF unstable regime, we have shown the existence of standing waves, heteroclinic connections between fixed points and between limit cycles, and some other patterns having different translation symmetries. We have focused our study on the heteroclinic orbits between fixed points or limit cycles which are spatially shifted by $L/4$. We have carried out a bifurcation analysis on a truncated version of the NCGLE restricted to the D_2 subspace to determine the regions of possible existence of heteroclinic orbits. Robust stability has been observed for the latter by means of simulations of the full NCGLE employing different initial conditions with noise. In brief, the main effects of increasing the range of the nonlocal interactions are the compression of the band of stable plane waves ($\alpha>0$, BF stable regime) or the creation of coherent structures out of turbulence that break diverse symmetries ($\alpha<0$, BF unstable regime) or turbulent structures with larger characteristic wavelengths.

ACKNOWLEDGMENTS

Financial support from the European Union (project DYNAMO, Contract No. 028669) and the excellence cluster Nanosystems Initiative Munich are gratefully acknowledged.

APPENDIX: DERIVATION OF THE NONLOCAL KERNEL FOR 1D ELECTROCHEMICAL SYSTEMS

Under static conditions, the electric potential in the electrolyte, $\phi(x,z)$ [15,17] obeys to a very good approximation Laplace's equation

$$\nabla^2\phi(x,z)=0. \tag{A1}$$

If we introduce the scale transformation $z\to Lz$, the boundary conditions are specified as

$$\phi(x,0)=F(x)=U-\phi_{DL}(x)\equiv\phi(x), \tag{A2}$$

$$\phi(x,\beta)=0, \tag{A3}$$

where $F(x)$ is a periodic function that satisfies $F(x+L)=F(x)$. If we Fourier transform both sides of Eq. (A1) on dimension x, we can define $\phi^{(u)}(z)\equiv\frac{1}{\sqrt{2\pi}}\lim_{L\to\infty}\int_{-L}^{L}\phi(x,z)e^{-iux/L}dx$ and the general solution of the resulting equation in Fourier space

$$\partial_z^2\phi^{(u)}-u^2\phi^{(u)}=0 \tag{A4}$$

is given by

$$\phi^{(u)}(z)=g_1(u)e^{uz}+g_2(u)e^{-uz}, \tag{A5}$$

where $g_1(u)$ and $g_2(u)$ are functions to be determined from Eqs. (A2) and (A3) in Fourier space. By applying the latter

and defining $F^{(u)} \equiv \frac{1}{\sqrt{2\pi}} \lim_{L\to\infty} \int_{-L}^{L} F(x) e^{-iux/L} dx$ we obtain

$$g_1(u) = \frac{F^{(u)}}{1 - e^{2u\beta}}, \tag{A6}$$

$$g_2(u) = -g_1(u) e^{2u\beta}, \tag{A7}$$

$$\phi^{(u)}(z) = -F^{(u)} \frac{\sinh[u(z-\beta)]}{\sinh[u\beta]}. \tag{A8}$$

By transforming Eq. (A8) back to physical space, we obtain

$$\phi(x,z) = \int_{-\infty}^{\infty} G(x-x',z) F(x') dx' = \int_{-\infty}^{\infty} G(x-x',z) \phi(x') dx', \tag{A9}$$

where $G(x-x',z)$ is the Green function for this geometry given by [18]

$$G(x-x',z) = -\frac{1}{2\beta} \frac{\sin\left[\frac{\pi(z-\beta)}{\beta}\right]}{\cos\left[\frac{\pi(z-\beta)}{\beta}\right] + \cosh\left[\frac{\pi(x-x')}{\beta}\right]}. \tag{A10}$$

As shown in [18]

$$\lim_{z\to 0^+} \frac{\partial G(x-x',z)}{\partial z} = \frac{\pi}{4\beta^2 \sinh^2\left(\frac{\pi(x-x')}{2\beta}\right)}, \tag{A11}$$

$$-\int_{-\infty}^{\infty} \lim_{z\to 0^+} \frac{\partial G(x-x',z)}{\partial z} dx' = \frac{1}{\beta}, \tag{A12}$$

if we use Eqs. (A2) and (A9) we can rewrite Eq. (6) as

$$\begin{aligned} i_{\text{mig. coupling}} &= -\sigma \left(\frac{\partial \phi}{\partial z} + \frac{\phi}{\beta}\right)\Bigg|_{z_{WE}} \\ &= -\sigma \int_{-\infty}^{\infty} \left[\lim_{z\to 0^+} \frac{\partial G(x-x',z)}{\partial z} \phi(x') + \frac{\delta(x-x')}{\beta} \phi(x) \right] dx' \\ &= -\sigma \int_{-\infty}^{\infty} \lim_{z\to 0^+} \frac{\partial G(x-x',z)}{\partial z} [\phi(x') - \phi(x)] dx' \\ &= \sigma \int_{-\infty}^{\infty} H_\beta(|x-x'|)[\phi_{DL}(x') - \phi_{DL}(x)] dx', \end{aligned}$$

with

$$H_\beta(|x-x'|) = \frac{\pi}{4\beta^2 \sinh^2\left(\frac{\pi(x-x')}{2\beta}\right)} + \frac{\delta(|x-x'|)}{\beta}. \tag{A13}$$

[1] Y. Kuramoto, *Chemical Oscillations, Waves and Turbulence*, Springer Series in Synergetics (Springer, Berlin, 1984).
[2] I. S. Aranson and L. Kramer, Rev. Mod. Phys. **74**, 99 (2002); M. C. Cross and P. C. Hohenberg, *ibid.* **65**, 851 (1993).
[3] B. I. Shraiman, A. Pumir, W. van Saarloos, P. C. Hohenberg, H. Chaté, and M. Holen, Physica D **57**, 241 (1992).
[4] N. Bekki and K. Nozaki, Phys. Lett. **110A**, 133 (1985).
[5] W. van Saarloos and P. C. Hohenberg, Physica D **56**, 303 (1992).
[6] M. van Hecke, Phys. Rev. Lett. **80**, 1896 (1998).
[7] H. Levine and X. Zou, Phys. Rev. Lett. **69**, 204 (1992); G. Veser, F. Mertens, A. Mikhailov, and R. Imbihl, *ibid.* **71**, 935 (1993); F. Mertens, R. Imbihl, and A. Mikhailov, J. Chem. Phys. **99**, 8668 (1993); F. Mertens, R. Imbihl, and A. Mikhailov, *ibid.* **101**, 9903 (1994); M. Falcke and H. Engel, *ibid.* **101**, 6255 (1994); M. Falcke, H. Engel, and M. Neufeld, Phys. Rev. E **52**, 763 (1995).
[8] R. Imbihl, Prog. Surf. Sci. **44**, 185 (1993).
[9] C. Josserand, Y. Pomeau, and S. Rica, Eur. Phys. J. Spec. Top. **146**, 47 (2007).
[10] Y. Kuramoto, Prog. Theor. Phys. **94**, 321 (1995).
[11] D. Tanaka and Y. Kuramoto, Phys. Rev. E **68**, 026219 (2003).
[12] Y. Kuramoto, D. Battogtokh, and H. Nakao, Phys. Rev. Lett. **81**, 3543 (1998).
[13] D. M. Abrams and S. H. Strogatz, Phys. Rev. Lett. **93**, 174102 (2004).
[14] V. Garcia-Morales and K. Krischer, Phys. Rev. Lett. **100**, 054101 (2008).
[15] K. Krischer, in *Advances in Electrochemical Sciences and Engineering*, edited by D. M. Kolb and R. C. Alkire (Wiley-VCH, Weinheim, 2003), p. 89.
[16] H. Varela, C. Beta, A. Bonnefont, and K. Krischer, Phys. Rev. Lett. **94**, 174104 (2005).
[17] N. Mazouz, G. Flätgen, and K. Krischer, Phys. Rev. E **55**, 2260 (1997); F. Plenge, H. Varela, and K. Krischer, Phys. Rev. Lett. **94**, 198301 (2005).
[18] J. Christoph, PhD. thesis, Free University, Berlin, 1999, http://www.diss.fu-berlin.de/diss/receive/FUDISS_thesis_000000000254; J. Christoph *et al.*, J. Chem. Phys. **110**, 8614 (1999).
[19] N. Mazouz *et al.*, J. Phys. Chem. B **101**, 2403 (1997); M. T. M. Koper and J. H. Sluyters, J. Electroanal. Chem. Interfacial Electrochem. **303**, 73 (1991); M. T. M. Koper, Electrochim. Acta **37**, 1771 (1992); F. Plenge, Y.-J. Li, and K. Krischer, J. Phys. Chem. B **108**, 14255 (2004).
[20] S. M. Cox and P. C. Matthews, J. Comput. Phys. **176**, 430 (2002).
[21] M. Golubitsky, I. Stewart, and D. G. Schaeffer, *Singularities*

and Groups in Bifurcation Theory: Volume II (Springer-Verlag, Berlin, 2000).
[22] D. J. B. Lloyd, A. R. Champneys, and R. E. Wilson, Physica D **204**, 240 (2005).
[23] R. Hoyle, *Pattern Formation: An Introduction to Methods* (Cambridge University Press, Cambridge, England, 2006).
[24] B. P. Luce, Physica D **84**, 553 (1995).
[25] E. J. Doedel, *AUTO, Software for Continuation and Bifurcation Problems in Ordinary Differential Equations*, http://indy.cs.concordia.ca/auto/
[26] D. Armbruster, J. Guckenheimer, and P. Holmes, Physica D **29**, 257 (1988).
[27] J. Guckenheimer, Physica D **20**, 1 (1986).
[28] I. G. Kevrekidis, B. Nicolaenko, and J. C. Scovel, SIAM J. Appl. Math. **50**, 760 (1990); D. Armbruster, J. Guckenheimer, and P. Holmes, *ibid.* **49**, 676 (1989).
[29] J. Lega, Physica D **152-153**, 269 (2001).
[30] S. Popp, O. Stiller, I. Aranson, A. Weber, and L. Kramer, Phys. Rev. Lett. **70**, 3880 (1993).
[31] P. Manneville and H. Chaté, Phys. Lett. A **171**, 183 (1992); H. Sakaguchi, Prog. Theor. Phys. **85**, 417 (1991).